Heliyon 9 (2023) e17601

Contents lists available at ScienceDirect

Heliyon

journal homepage: www.cell.com/heliyon

Triethylammonium salt of a synthesized dicoumarol: Structural insight and human anti-glioblastoma activities

Afzal Khan [a,b,c], Muhammad Ikram [a,*], Sadia Rehman [a,**], Rizwan Khan [d], Vinay K. Puduvalli [d], Ayub Jadoon [b], Momin Khan [a], Fawaz Alasmari [e], Abdullah F. AlAsmari [e]

[a] Department of Chemistry, Abdul Wali Khan University, Mardan, Pakistan
[b] Department of Microbiology, Abbotabad University of Science and Technology, Abbotabad, Pakistan
[c] Department of Neuro-Oncology, Division of Cancer Medicine, The University of Texas MD Anderson Cancer Center, Houston, TX, USA
[d] Department of Zoology, Abdul Wali Khan University, Mardan, Pakistan
[e] Department of Pharmacology and Toxicology, College of Pharmacy, King Saud University, Riyadh 11451, Saudi Arabia

ARTICLE INFO

Keywords:
Dicoumarol
Dicoumarol triethylammonium salt
Glioblastoma
Flow cytometry
Phase contrast microscopy
Free radical scavenging

ABSTRACT

Glioblastoma multiforme (GBM) is the most common and primary brain tumor with poor prognosis. They are removed by following tedious and life threatening surgeries. GBM stem cells (GSCs) are the main source of tumor recurrence after surgery. Hence, drugs are designed to overcome the recurrent glioblastoma malignant cells. Currently used chemotherapies are not cost effective as well as bear resistance. New and effective chemotherapeutic compounds are developed to overcome the intrinsic and acquired resistance. Dicoumarol derivative 3,3′-[(4-methoxyphenyl)methanediyl]bis(4-hydroxy-2Hchromen-2-one) (HL) and its triethylammonium salt triethylammonium3-[(4-methoxyphenyl)(4-hydroxy-2-oxo-2H-chromen-3-yl)methyl]-2-oxo-2H-chromen-4-olate (L) were synthesized and characterized using spectral and analytical techniques. The deprotonated compound L was further studied structurally using single crystal analysis. Cytotoxic studies against human glioblastoma cells A172 and LN229 were investigated both dose and time dependently and compared with the cytotoxicity of normal human astrocytes (NHA). The IC_{50} value of HL against A172 was found to be lying within the range 2.68–0.95 μM whereas against LN229 the range was found to be 9.55–0.85 μM. Similarly, the compound L revealed range of 1.9–0.271 μM against A172 and 1.2–0.27 μM against LN229. Cell cycle arrest was observed in GBM cells treated with L compared to the control group, which suggested that L may trigger apoptosis in GBM cells according to cytotoxicity and flow cytometry results. The antioxidant activity of synthesized compounds was also investigated using DPPH free radicals.

1. Introduction

Malignant tumors are serious illnesses with significant morbidity and mortality rates in adults. They are the second largest cause of cancer deaths in children [1]. Glioblastoma multiforme (GBM) is the most common and life-threatening malignant primary brain

* Corresponding author.
** Corresponding author.
E-mail addresses: ikram@awkum.edu.pk (M. Ikram), sadia@awkum.edu.pk (S. Rehman).

https://doi.org/10.1016/j.heliyon.2023.e17601
Received 30 May 2023; Received in revised form 18 June 2023; Accepted 22 June 2023
Available online 25 June 2023

tumor in adults. Furthermore, GBM has a recurrence rate of more than 90%, even following multimodal treatment that combines surgery and chemotherapy [2]. Moreover, the most effective treatment for GBM at the moment, temozolomide (TMZ), is becoming less effective because to the emergence of chemo resistance, which leads to poor clinical outcomes [3]. However, it is essential to use novel therapeutic approaches for gliomas.

Coumarin and its derivatives are among the most active classes of compounds, with a wide range of biological actions [4–7]. Many of these compounds have proven to be active as antibacterial [8]. Coumarins have a wide range of pharmacological effects, including anti-diabetic, anti-viral, anti-microbial, anticancer, anti-oxidant, anti-parasitic, anti-helminthic, and anti-proliferative, anti-convulsant, anti-inflammatory, antihypertensive properties, antifungal [9], anti-HIV [10] and antitumor agents [11]. Numerous cancer cell lines have been shown to experience a reduction in cell proliferation when exposed to certain coumarin compounds, such as coumarin and 7-hydroxycoumarin [12–14].

Among the most intriguing developments in the field of medicinal drugs, coumarins are playing very important role in various biological activities viz; warfarin, a derivative of dicoumarol is used as coagulant, novobiocin is used as antibacterial agent etc [15,16]. Inspired by this our present study focuses on the exploration of anti-glioblastoma activities of the two synthesized compounds. Novel approaches were, therefore, adopted to treat this deadly disease including the development of dicoumarol as therapeutic agent for the possible treatment of glioblastoma. So far, no scientific report has been published regarding the use of dicoumarol as antiglioblastoma agent. Condensation of 4-methoxybenzaldehyde with 4-hydroxycoumarin produced the 3,3′-[(4-methoxyphenyl)methanediyl]bis (4-hydroxy-2Hchromen-2-one) (HL) which was subsequently deprotonated using triethylamine as deprotonating agent and as a result triethylammonium3-[(4-methoxyphenyl)(4-hydroxy-2-oxo-2H-chromen-3-yl)methyl]-2-oxo-2H-chromen-4-olate (L) is produced. Both the compounds were studied structurally using different spectroscopic techniques. It was hypothesized that the deprotonated salt of dicoumarol may possess better chemotherapeutic effects than its non-deprotonated parent compound. And our hypothesis was proved by the positive results shown by triethylammonium3-[(4-methoxyphenyl)(4-hydroxy-2-oxo-2H-chromen-3-yl) methyl]-2-oxo-2H-chromen-4-olate (L) against LN229 and A172 glioblastoma.

Scientific evidence reveals that antioxidants reduce the risk of chronic diseases such as cancer and heart disease [17]. Antioxidants can protect cellular organelles from free radical-induced oxidative stress. Hydroxyl radicals, superoxide anion radicals, and hydrogen peroxide are among the free radicals produced endogenous inside biological system. Highly reactive free radicals produced by external substances, anxiety, or the food system can oxidize biomolecules, resulting in cancer, coronary heart disease, and hypertension [17]. Therefore, scavenging free radicals is also one of the strategies to counter cancers. Previously coumarin-benzimidazole hybrid compounds were studied for their anticancer, antioxidant, anticonvulsant, and carbonic anhydrase inhibitory properties [18]. Hence the main objective of this study will be (i) anticancer activity of coumarin derivatives in glioma cell lines and (ii) free radicals scavenging properties of the synthesized compounds using DPPH free radicals.

2. Material and method

2.1. Chemicals and reagents

A well-optimized technique was used to synthesize a dicoumarol derivative and the chemicals were purchased from local suppliers. Trypan blue was purchased from Sigma Chemical Co. (St. Louis, MO, USA). Merck Co. provided potassium phosphates and dimethyl sulfoxide (DMSO) (Darmstadt, Germany). DMEMF-12 5050,1X (Dulbecco's Modification of Eagle's Medium Ham's F-12 5050 Mix) Gibco BRL provided WIL-glutamine, PBS, 1X (Phosphates-buffered saline) without calcium and magnesium, fetal bovine serum (FBS), penicillin-streptomycin, trypsin-EDTA, and glutamine (Grand Island, NY14072, USA).

2.2. Instrumentation

The characterization of the dicoumarol and its salt was carried out using different instruments. The percent elemental composition (experimental) was obtained by using a Varian Elementar II instrument. IR spectra of the compounds were recorded on a PerkinElmer spectrophotometer version 10.4.00 with serial number 95120 made in Lliantrisant, UK. A BRUKER advance III 400 spectrometer was used to record the ^{1}H-NMR and ^{13}C-NMR spectra of the compounds.

2.3. Crystal structure determination

Crystals of the triethylammonium3-[(4-methoxyphenyl)(4-hydroxy-2-oxo-2H-chromen-3-yl)methyl]-2-oxo-2H-chromen-4-olate (L) were mounted on a glass fibre in inert paraffin oil. Data were recorded at 170 K on a STOE-IPDS 2T diffractometer with graphite-monochromated Mo-K_{α}-radiation ($\lambda = 0.71073$ Å). The program X-area was used for integration of diffraction profiles; numerical absorption corrections were carried out with the programs X-Shape and X-Red32; all from STOE©. The structures were solved by dual space methods (SHELXT-2015) [19] and refined by full-matrix least-squares techniques using the WingX GUI [20] and SHELXL-2015 [21]. All non-hydrogen-atoms were refined with anisotropic displacement parameters. The hydrogen atoms were refined isotropically on calculated positions using a riding model with their U_{iso} values constrained to 1.5 U_{eq} of their pivot atoms for terminal sp^3 carbon atoms and 1.2 times for all other carbon atoms. Crystallographic details are supplied in the supplementary information file and the structure was submitted to the CCDC. Data can be obtained free of charge from the Cambridge Crystallographic Data Centre by FAX (+44-1223-336-033), email (deposit@ccdc.cam.ac.uk) or their web interface (at http://www.ccdc.cam.ac.uk) by quoting the CCDC-number **2232189** for L.

2.4. Biological studies

2.4.1. Cell culture

The human brain tumor cell lines A172, LN229, and NHA were obtained from MD Anderson Research Cancer Center and immediately placed in a 10-cm^3 tissue culture plate with MEM medium supplemented with 10% FBS, 100 U/ml penicillin, 100 g/mL streptomycin, and 1% glutamine, and grown at 37 °C in a humidified 5% CO_2 and 95% air atmosphere.

2.4.2. Cell viability

The WST technique was used to evaluate cell viability. The A172, LN229, and NHA cells were seeded in 96-well plates at a density of 3×10^3 cells/well and incubated at 37 °C for 24 h. Various concentrations of coumarin (0.16, 0.8, 4, 20, and 100 μM) were subjected to the cells and cultured for varying amounts of time. The control regimen included the use of DMSO (solvent). After that, the cell lines were cultured with WST-1 reagent according to the manufacturer's instructions. Cells were incubated for 4 h at 37 °C in a humidified incubator with 5% CO_2. Absorbance was measured using a 516 nm test wavelength and a 600 nm reference wavelength. The proportion of viable cells in each group is calculated for untreated control cells [22]. Cell morphology was investigated and photographed using a phase-contrast microscope [23].

2.4.3. Flow cytometry analysis of cell cycle and apoptosis

Approximately 1×10^6 cells/in 10 cm^3 plates were incubated with concentrations (4,10 μM) of coumarin for 0, 24,48, and 72 h before the cells were harvested by centrifuging and washed by PBS, fixed with chilled 70% ethanol for 12 h at night. Flow cytometry was employed in cells after staining with propidium iodide (PI) to examine the apoptosis and cell cycle arrest. The cell cycle distribution (G0/G1, S, and G2/M phase) was analyzed by Multi-Cycle Software [24].

2.4.4. 2,2-Diphenyl-1-picrylhydrazyl) (DPPH) radical scavenging studies

The DPPH radical scavenging activities of the synthesized dicoumarol and its salt were evaluated using method reported by Soare, Dinis, Cunha, & Almeida, 1997 [25]. Initially, 0.1 mL of each sample at 250, 500, 750, and 1000 g/mL concentrations was mixed with 1 mL of 0.2 mM DPPH dissolved in methanol. The reaction mixture was incubated at 28 °C in the dark for 20 min. The control contained all the chemicals but no sample, whereas methanol served as a blank. The absorbance at 517 nm was measured using a UV/Vis spectrophotometer to evaluate the DPPH radical scavenging activity. Ascorbic acid's DPPH radical scavenging activity was also measured for comparison.

The percentage of DPPH radical scavenger was calculated using Equation (1).

$$DPPH\ Inhibition\ effect\ (\%) = \frac{A_C - A_S}{A_C} \times 100 \quad (1)$$

where, A_c = Absorbance reading of the control and A_s = Absorbance reading of the sample.

2.4.5. Statistical analysis

All in vitro experiments were conducted at least 3 times independently and statistical analysis was performed using unpaired Student's *t*-test for at least three independent experiments. Differences at $P < 0.05$ were considered statistically significance.

2.5. Synthesis of 3,3'-[(4-methoxyphenyl)methanediyl]bis(4-hydroxy-2Hchromen-2-one) (HL)

3,3′-[(4-methoxyphenyl)methanediyl]bis(4-hydroxy-2H-chromen-2-one) was synthesized following essentially the reported procedure [26]. 25 mmol of the 4-methoxybenzaldehyde was added to the 50 mmol stirred ethanolic solution of 4-hydroxycoumarin and the mixture was refluxed for 3 h at 120 °C. After cooling the reaction mixture, solid white powder of the HL were isolated, washed several times with copious 10% ethanolic *n*-hexane solution. The product was purified by dissolving in methanolic solution. The process repeated two times to get pure recrystalised dicoumarol compound.

IR: 2800(w), 1650(s), 1602(s), 1558(s), 1506(s), 1448(w), 1352(s), 1305(s), 1257(s), 1176(s), 1093(s), 1053(s), 960(s), 904(s), 767(s), 673(s) cm^{-1}, ^{1}H NMR (400.23 MHz, $(CD_3)_2OS$, 303 K) (δ, ppm): 3.5 (s, 3H, OCH_3); 6.23 (s, 1H, C12), 6.75–7.85 (m, H-aromatic), 10.01 (s, 1H, OH); $^{13}C\{^1H\}$-NMR (150.9 MHz, $(CD_3)_2OS$) (δ, ppm): 54.87 (CH_3, –OCH_3), 103.78 (CH, C12), 112.12–131.33 (C, Caromatic), 152.18 (C4,C18), 169.70 (C2,C14), Elemental Analysis ($C_{26}H_{18}O_7$), Calc. C: 70.58%, H: 4.10%, Exp. C: 70.80%, H: 4.92%, EI-MS: *m/z* (%) 441.0974 (100%) [$C_{26}H_{17}O_7$–H^+].

2.6. Synthesis of triethylammonium3-[(4-methoxyphenyl)(4-hydroxy-2-oxo-2H-chromen-3-yl)methyl]-2-oxo-2H-chromen-4-olate (L)

The subsequent deprotonation of 3,3′-[(4-methoxyphenyl)methanediyl]bis(4-hydroxy-2H-chromen-2-one) was carried out by adding 1 mL of triethylamine to its methanolic solution. The resulting transparent yellowish solution was left standing overnight to grow transparent crystals of triethylammonium-3-[(4-methoxyphenyl)(4-hydroxy-2-oxo-2H-chromen-3-yl)methyl]-2-oxo-2H-chromen-4-olate (L). IR: 3369(s), 3203(bd), 1639(s), 1616(s), 1558(s), 1506(s), 1489(s), 1456(s), 1361(s), 13,010(s), 1273(s), 1236(s), 1201(s), 1153(s), 1099(s), 1028(s), 968(s), 926(s), 906(s), 862(s), 819(s),746(s), 721(s), 696(s), 648(s) cm^{-1}, ^{1}H-NMR (400.23 MHz, $(CD_3)_2OS$, 303 K) (δ, ppm): 1.06 (t, 3H, $\underline{CH_3}$–CH_2–N), 2.67 (s, 1H, NH), 3.43 (q, 2H, CH_3–$\underline{CH_2}$–N), 3.83 (s, 3H, OCH_3),

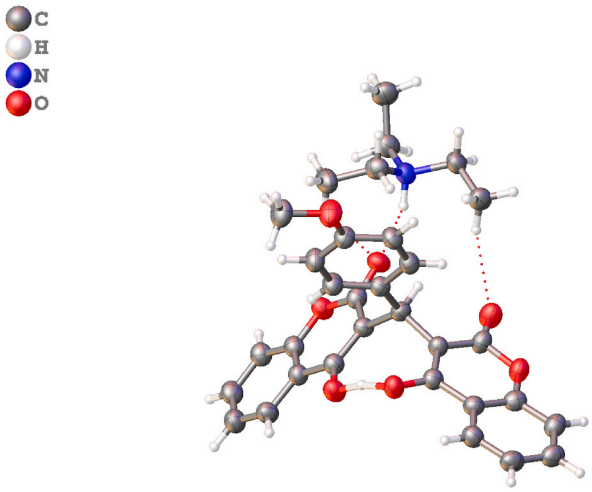

Fig. 1. Molecular structure of triethylammnium 3-[(4-methoxyphenyl)(4-hydroxy-2-oxo-2H-chromen-3-yl)methyl]-2-oxo-2H-chromen-4-olate (L). Ellipsoids are shown at the 50% probability level.

Table 1
Crystal data and structure refinement parameters for triethylammonium3-[(4-methoxyphenyl)(4-hydroxy-2-oxo-2H-chromen-3-yl)methyl]-2-oxo-2H-chromen-4-olate (L).

Compound	L
Empirical formula	$C_{26}H_{17}O_7^-\cdot C_6H_{16}N^+$
Formula mass	543.59
Temperature	170 K
Wavelength	0.71073 Å
Crystal system, space group	Monoclinic, $P2_1/n$
Unit cell dimensions	$a = 10.614$ (2) Å $b = 17.633$ (4) Å $c = 14.178$ (3) Å β = 93.00 (3)°
Volume	2649.8 (9) $Å^3$
Crystal size (mm)	0.21 × 0.13 × 0.13 mm
Z, Calculated density	1.363 Mg m^{-3}
Absorption coefficient	0.10 mm^{-1}
F(000)	1152
Θ range for data collection	6.2–59.0°
Limiting indices	$h = -13 \rightarrow 11$, $k = -22 \rightarrow 22$ $l = -17 \rightarrow 17$
Measured reflections	20,325
Independent reflections	5395
Reflections with I > 2σ(I)	2060
R_{int}	0.145
Refinement method	Full-matrix least-squares on F^2
Data/restraints/parameters	53,950/373
$R[F^2 > 2\sigma(F^2)]$	0.058

6.41 (s, 1H, C12), 7.30–8.90 (m, H-aromatic), 8.09 (s, 1H, OH); $^{13}C\{^1H\}$-NMR (150.9 MHz, $(CD_3)_2OS$) (δ, ppm): 15.49 (CH_3, $\underline{CH_3}$–CH_2–N), 47.36 (CH_2, CH_3–$\underline{CH_2}$–N), 102.47 (CH_3, –OCH_3), 103.70 (CH, C12), 116.57–145.55 (C, Caromatic), 153.52 (C4,C18), 164.84, 168.81 (C2,C14), Elemental Analysis ($C_{26}H_{17}O_7^-\cdot C_6H_{16}N^+$), Calc. C: 71.91%, H: 6.17%, N: 2.62% Exp. C: 72.34%, H: 6.10%, N: 2.32%.

3. Result and discussion

Condensation of 4-methoxybenzaldehyde with 4-hydroxycoumarin produced the 3,3′-[(4-methoxyphenyl)methanediyl]bis(4-hydroxy-2Hchromen-2-one) (HL). The compound is unique due to strong intramolecular hydrogen bonding arising from the dicoumarol structure. The compound was characterized through solid ATR analysis, ^{1}H-NMR, $^{13}C\{^1H\}$-NMR and ESI(+) mass analysis. The percent abundance was seen to be in coincidence with the corresponding molecular ion peak at 441.0974.^{1}H and $^{13}C\{^1H\}$-NMR spectra shown peaks at 3.72 assigned to the methoxy group attached to the phenyl ring. Whereas two singlets were observed each assigned to CH of

Table 2
Selected bond lengths and bond angles for triethylammonium3-[(4-methoxyphenyl)(4-hydroxy-2-oxo-2H-chromen-3-yl)methyl]-2-oxo-2H-chromen-4-olate (L).

Selected bond lengths			
Moiety	Bond Length, Å	Moiety	Bond Length, Å
O1–C3	1.221 (4)	N1–C31	1.499 (4)
O2–C4	1.378 (4)	N1–C29	1.505 (5)
O2–C3	1.400 (4)	N1–C27	1.505 (4)
O3–C10	1.301 (4)	N1–H1N	0.96 (4)
O4–C12	1.233 (4)	O7–C23	1.379 (4)
O5–C13	1.377 (4)	O7–C26	1.435 (4)
O5–C12	1.386 (4)	C1–C2	1.518 (5)
O6–C19	1.307 (4)	C1–C11	1.519 (5)
C1–C20	1.532 (5)	C1–H1	1.0000
Selected bond angles			
Moiety	**Bond angle,** °	**Moiety**	**Bond angle,** °
C4–O2–C3	120.8 (3)	C22–C23–O7	124.1 (3)
C13–O5–C12	121.0 (3)	O7–C23–C24	115.7 (3)
C23–O7–C26	116.9 (3)	O2–C4–C9	121.1 (3)
O1–C3–O2	113.7 (3)	O2–C4–C5	116.4 (3)
O1–C3–C2	127.1 (3)	O3–C10–C2	122.9 (3)
O2–C3–C2	119.3 (3)	O3–C10–C9	118.2 (3)
O7–C26–H26C	109.5	O4–C12–O5	113.0 (3)
C31–N1–C29	113.5 (3)	O4–C12–C11	127.0 (4)
C31–N1–C27	111.9 (3)	O5–C12–C11	119.9 (3)
C29–N1–C27	110.9 (3)	O5–C13–C18	120.7 (3)
C31–N1–H1N	102 (2)	O5–C13–C14	116.6 (3)
C29–N1–H1N	111 (3)	N1–C29–C30	114.7 (3)
C27–N1–H1N	107 (2)	O6–C19–C11	124.3 (3)
C28–C27–N1	113.1 (3)	O6–C19–C18	116.0 (3)
N1–C31–C32	112.6 (3)	N1–C31–H31B	109.1

the bonded phenoxy ring to the 4-hydroxycoumarin and OH of the 4-hydroxycoumarin. Rest of the spectrum was comprised exclusively of the signals for aromatic protons. $^{13}C\{^{1}H\}$-NMR is establishing the correct assignments of the corresponding peaks to their carbon nuclei [26]. ATR spectrum of the HL reveals representative band at 1650 cm^{-1} which corresponds to the carbonyl stretching frequency in case of dicoumarol type of bonding between the lactone and hydroxyl groups.

A band at 1093 cm^{-1} assigned to the stretching vibration of lactone ring. Hydroxyl vibrations were not observed due to their involvement in strong intramolecular hydrogen bonding. Dicoumarols are very active molecular units and have been tested in many biological applications but due to this unique hydrogen bonding, dicoumarols are rendered to be somehow hydrophobic in biological fluids and thereby decreasing their efficiency. The strong hydrogen bonding was established and studied by many workers around the globe [27]. It was hypothesized that increasing hydrophilicity may pave the way to develop coumarin based antiproliferative agent against human glioblastoma. Therefore, the parent dicoumarol 3,3′-[(4-methoxyphenyl)methanediyl]bis(4-hydroxy-2Hchromen-2-one) was converted to its triethylammonium salt triethylammonium3-[(4-methoxyphenyl)(4-hydroxy-2-oxo-2H-chromen-3-yl)methyl]-2-oxo-2H-chromen-4-olate (L) being the fifth of its kind. It was characterized crystallographically using the single crystal diffraction analysis and solid-state ATR.

3.1. Molecular structure of triethylammonium3-[(4-methoxyphenyl)(4-hydroxy-2-oxo-2H-chromen-3-yl)methyl]-2-oxo-2H-chromen-4-olate (L)

The molecular structure of the deprotonated triethylammnium 3-[(4-methoxyphenyl)(4-hydroxy-2-oxo-2H-chromen-3-yl)methyl]-2-oxo-2H-chromen-4-olate (L) is shown in Fig. 1 and the crystal data is given in Table 1.

The charge assisted hydrogen bonding (-CAHB) produced after the deprotonation of the one of the hydroxy-coumarin moiety not the other is negligibly shorter than{*D* … *A* = 2.415(4) Å} than similar bond length reported in triethylammonium 3-[(4-hydroxy-3-methoxyphenyl)(4-hydroxy-2-oxo-2H-chromen-3-yl)methyl]-2-oxo-2H-chromen-4-olate, $C_6H_{16}N^+.C_{26}H_{17}O_8$ {*D* … *A* = 2.413(15) Å} [28]. Similar charge assisted intramolecular hydrogen bonding had been rarely reported though not unprecedented [27–29]. The *D*–H···*A* = 169 (4)° for -CAHB in triethylammonium3-[(4-methoxyphenyl)(4-hydroxy-2-oxo-2H-chromen-3-yl)methyl]-2-oxo-2H-chromen-4-olate while the distance of the freely refined hydrogen atom to its parent atom O6 is rather short by 1.11(5)Å comparatively lower in value to its close counterpart reported earlier [28]. The short distances *D*–H···*A* and *D* … *A* leads to strong intramolecular hydrogen bonding and hence forms an eight membered ring (C10/O3/H6O/O6/C19/C11/C1/C2). The strong intramolecular hydrogen bonding also affects other bond distances viz; the bond length for the bound alcoholic oxygen atoms to the carbon vary in the range 1.301 (4)Å to 1.307 (4) Å. Both the bond lengths being very similar are significantly shorter than those reported for non-deprotonated derivatives. The values for the bond lengths in both the alcoholic moieties are in accordance with protonated and deprotonated to a certain extent as was found in triethylammonium 3-[(4-hydroxy-3-methoxyphenyl)(4-hydroxy-2-oxo-2H-chromen-3-yl)methyl]-2-oxo-2H-chromen-4-olate, $C_6H_{16}N^+.C_{26}H_{17}O_8^-$ [28].

Table 3
Hydrogen-bond parameters triethylammonium3-[(4-methoxyphenyl)(4-hydroxy-2-oxo-2H-chromen-3-yl)methyl]-2-oxo-2H-chromen-4-olate (L).

D–H···*A*	*D*–H	H···*A*	*D*···*A*	*D*–H···*A*
C14–H14···O1[i]	0.95	2.38	3.250 (5)	152
O6–H6*O*···O3	1.11 (5)	1.32 (5)	2.415 (4)	169 (4)
C27–H27*A*···O3[ii]	0.99	2.54	3.333 (5)	137
C28–H28*C*···O1	0.98	2.51	3.427 (5)	155
C29–H29*A*···O7[iii]	0.99	2.26	3.140 (5)	148
C29–H29*B*···O6[ii]	0.99	2.60	3.376 (5)	135
C32–H32*C*···O4	0.98	2.52	3.285 (5)	135
N1–H1*N*···O4	0.96 (4)	1.85 (4)	2.764 (4)	159 (4)

Symmetry codes: (i) $-x+1, -y+1, -z+1$; (ii) $x+1, y, z$; (iii) $x+1/2, -y+3/2, z-1/2$.

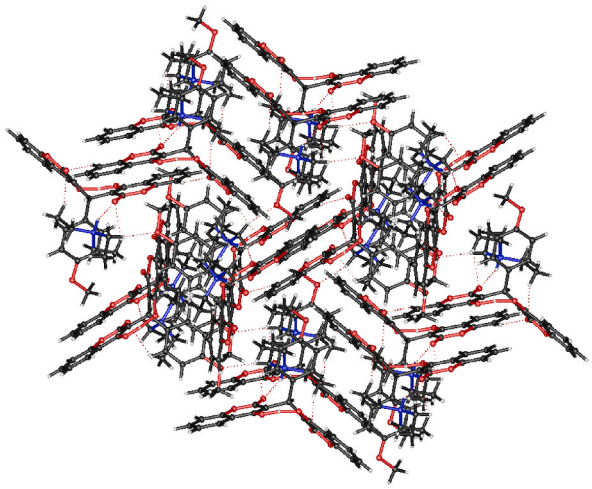

Fig. 2. Crystal packing diagram of triethylammnium 3-[(4-methoxyphenyl)(4-hydroxy-2-oxo-2H-chromen-3-yl)methyl]-2-oxo-2H-chromen-4-olate (L).

The deprotonating agent ammonium molecule also exhibit certain intermolecular hydrogen bonding with the lactone oxygen atoms. One of these intermolecular hydrogen bonding arises from moiety N1–H1*N*···O4 with *D* … *A* = 2.764 (4)Å and *D*–H···*A* = 159 (4)° pointing comparatively shorter parameters than found in close derivative. The other intermolecular hydrogen bonding is found between lactone oxygen O1 and H28*C* of the ammonium molecule. The metrical parameters for the intermolecular hydrogen bond (C28–H28*C*···O1) are *D* … *A* = 3.427 (5)Å and *D*–H···*A* = 155°.

The steric strain in the deprotonated triethylammonium3-[(4-methoxyphenyl)(4-hydroxy-2-oxo-2H-chromen-3-yl)methyl]-2-oxo-2H-chromen-4-olate may be clearly deduced from the C–C1–C bond angles around methine moiety (Table 2). C2–C1–C11 = 117.3 (3)°, C2–C1–C20 = 112.7 (3)° and C2–C1–C11 = 117.3 (3)° show that the bond angles around methine moiety are slightly widened compared to the ideal tetrahedral values. Most likely, the steric strain is involved in widening these angles. The bond lengths of the O–C moiety in the pyran ring reveal the trend viz; O2–C3 = 1.400 (4)Å, O2–C4 = 1.378 (4)Å, O5–C12 = 1.386 (4)Å and O5–C13 = 1.377 (4) Å establishes that the intramolecular hydrogen bonding arising from N1–H1N···O4 (Table 3) also impart effect on the O2–C3 bond lengths unlike the other similar bond lengths. The dihedral angle of 56.29° between the two planar benzopyran planes of C2/C3/O2/C4–C10, and C11/C12/O5/C13–C19 show greater deviation as reported in triethylammonium 3-[(4-hydroxy-3-methoxyphenyl)(4-hydroxy-2-oxo-2H-chromen-3-yl)methyl]-2-oxo-2H-chromen-4-olate. The two benzopyran planes are further lying at 76.76° and 75.93°, respectively to the plane produced by C20/C21/C22/C23/C24/C25.

The triethylammonium3-[(4-methoxyphenyl)(4-hydroxy-2-oxo-2H-chromen-3-yl)methyl]-2-oxo-2H-chromen-4-olate bears characteristics like dichromone arrangement of oxygen atoms where the carbonyl faces carbonyl, strong intramolecular hydrogen bonds and low symmetry for 4-methoxyphenyl substituent compared to the neutral molecule {C2–C1–C20–C21 = 169.45° and C11–C1–C20–C25 = 127.54°}.

The supramolecular structure of triethylammonium3-[(4-methoxyphenyl)(4-hydroxy-2-oxo-2H-chromen-3-yl)methyl]-2-oxo-2H-chromen-4-olate as shown in Fig. 2 reveals no parallel arrangement of the phenyl or benzopyran rings therefore, no π-π stacking exist. Rather the crystal packing is dominated by intermolecular hydrogen bonding. The methoxy oxygen atom O7 has been seen bridging the adjacent cation and anion by hydrogen acceptor in a non-classical hydrogen bonding { C29–H29A···O7[iii] ($x+1/2, -y+3/2, z-1/2$); *D*···*A* = 3.140 (5) Å which has been found comparatively stronger than similar hydrogen bonding reported earlier {O8···H27B–C27($-x+3/2, y+1/2, -z+3/2$); *D*···*A* = 3.257 (2) Å} [32]. Other hydrogen bonds which are involved in determining the supramolecular structure are (i) the classical N1–H1*N*···O4; *D*···*A* = 2.764 (4) Å and the (ii) non-classical C27–H27*A*···O3[ii]($x+1, y, z$);

(a)

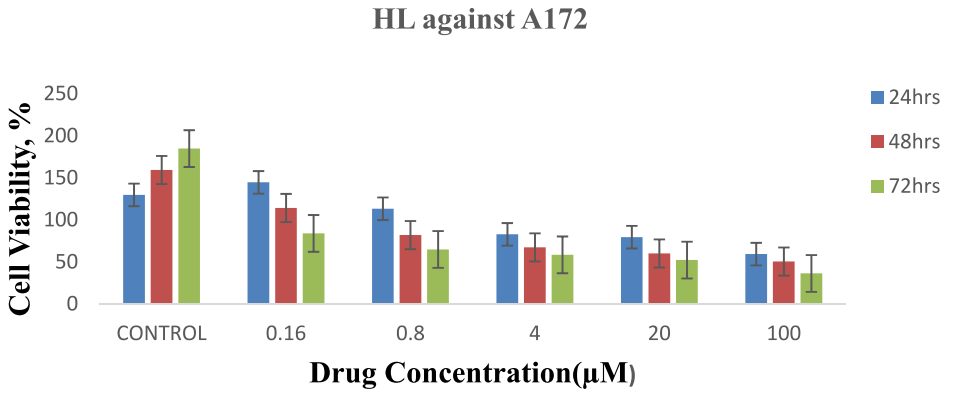

(b)

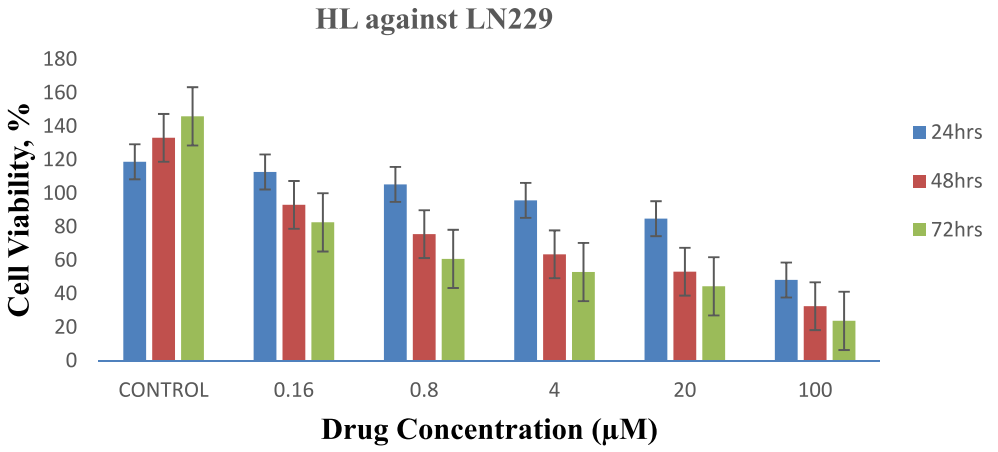

(c)

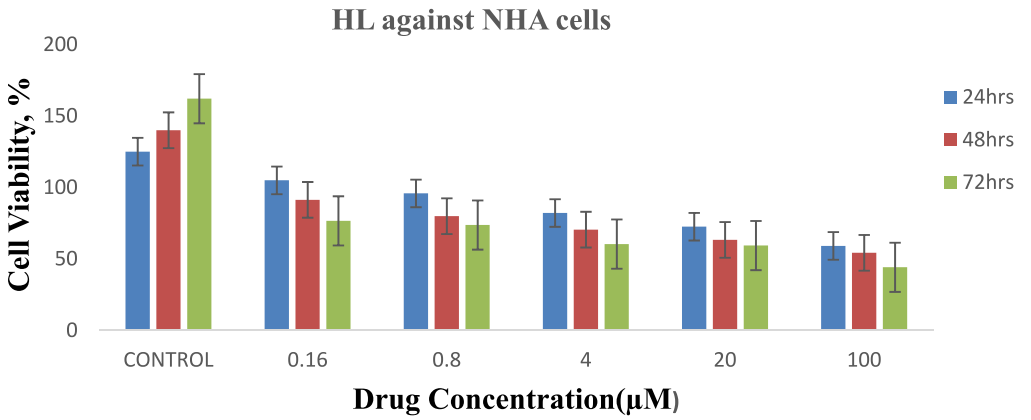

Fig. 3. Cytotoxicity of HL against human glioma cell growth. (a) HL against A172 cells (b) HL against LN229 cells and (c) HL against NHA cells (3000 cells/well) were seeded in 96-well plate, and cells were exposed to HL at different concentration (0, 0.16, 0.8, 4, 20,100 µM) for 24, 48,72 h. Methylprophyl tryptamine (200 nm) was used as the positive control. Cell viability was detected via WST.

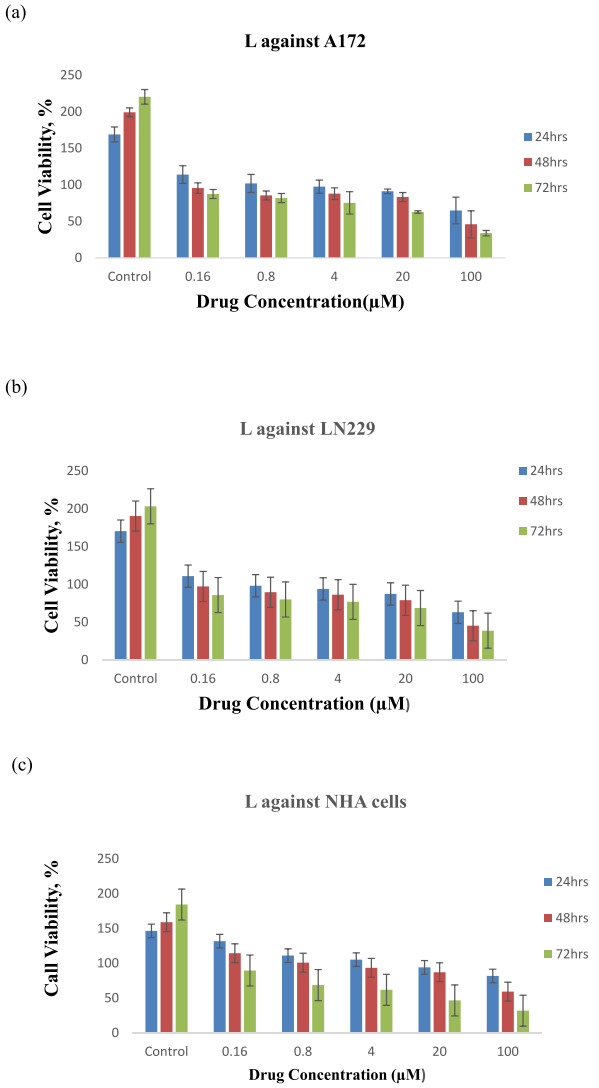

Fig. 4. Cytotoxicity of L against human glioma cell growth. (a) L against A172 cells (b) L against LN229 cells and (c) L against NHA cells (3000 cells/well) were seeded in 96-well plate, and cells were exposed to L at different concentration (0, 0.16, 0.8, 4, 20,100 μM) for 24, 48,72 h. Methylprophyl tryptamine (200 nm) was used as the positive control. Cell viability was detected via WST.

$D\cdots A$ = 3.333 (5) Å. The infinite flat chains of the benzopyrane rings are produced by other supported hydrogen bonding like C14–H14···O1^{i} ($-x+1$, $-y+1$, $-z+1$); $D\cdots A$ = 3.250 (5) Å. Overall the crystal packing of the molecule exhibit a zig zag helical type of arrangement along as shown in Fig. 2(b).

3.2. Anti-glioblastoma viability assay

The protonated dicoumarol 3,3′-[(4-methoxyphenyl)methanediyl]bis(4-hydroxy-2Hchromen-2-one) {HL} and its deprotonated salt triethylammonium3-[(4-methoxyphenyl)(4-hydroxy-2-oxo-2H-chromen-3-yl)methyl]-2-oxo-2H-chromen-4-olate (L) were studied for their antiproliferation activities using human glioblastoma cells LN229 and A172. Both derivatives were studied for their effects on both the tumor cell lines for a range of drug concentration (160 nM-100 μM; 0 μM corresponds to the control). The effect of the both tested compounds against star-shaped glial cells normal human astrocyte (NHA) was also tested and shown below in the form of graph. The results were compared with the already used drug methylprophyl tryptamine (MPT). Among the currently used chemotherapeutic agents, coumarin derivatives have been studied extensively against different types of human cancers. These studies include coumarin and its derivative against HL-60 (leukemia), MCF-7 (breast), A549 and H727 (lung) and ACHN (kidney) [12,30–32]. The clinical studies on metastatic renal cell carcinoma patients revealed that 14 of 45 RCC patients showed positive results with almost no toxic/side effects when coumarin or its derivatives was administered orally with the addition of cimetidine [33–35]. Hence, our study was predominantly focused on coumarin based drug development for the treatment of glioblastoma. Coumarin and its derivatives are also

Table 4
Cell viability results of HL and L. {MPT: Methylprophyl tryptamine}.

Compound	Time	Cell viability ($\overline{X}$ ±SD)					
		A172 cancerous cells					
		Control	0.16 μM	0.8 μM	4 μM	20 μM	100 μM
HL	After 24 h	129.6	144.6	113.2	82.80	79.44	59.25
	After 48 h	159.2	114.1	81.85	67.26	60.04	50.45
	After 72 h	184.7	83.86	64.81	58.42	52.18	36.29
		LN229 cancerous cells					
		Control	**0.16 μM**	**0.8 μM**	**4 μM**	**20 μM**	**100 μM**
	After 24 h	118.7	112.6	105.2	95.71	84.77	48.15
	After 48 h	133.1	93.00	75.52	63.49	53.09	32.49
	After 72 h	145.9	82.57	60.76	52.90	44.36	23.74
		NHA non-cancerous cells					
		Control	**0.16 μM**	**0.8 μM**	**4 μM**	**20 μM**	**100 μM**
	After 24 h	125.0	104.9	95.80	82.08	72.52	59.10
	After 48 h	139.9	91.31	79.89	70.47	63.29	54.27
	After 72 h	162.0	76.62	73.69	60.37	59.34	44.11
L		**A172 cancerous cells**					
		Control	**0.16 μM**	**0.8 μM**	**4 μM**	**20 μM**	**100 μM**
	After 24 h	168.8	113.9	101.8	97.42	91.18	64.87
	After 48 h	199.1	95.46	85.43	87.86	83.27	45.93
	After 72 h	220.3	87.39	81.86	75.29	62.76	33.83
		LN229 cancerous cells					
		Control	**0.16 μM**	**0.8 μM**	**4 μM**	**20 μM**	**100 μM**
	After 24 h	170.4	110.8	98.11	93.94	87.33	63.10
	After 48 h	190.3	97.21	89.56	86.34	79.04	45.27
	After 72 h	203.2	85.85	80.05	76.84	68.72	38.75
		NHA non-cancerous cells					
		Control	**0.16 μM**	**0.8 μM**	**4 μM**	**20 μM**	**100 μM**
	After 24 h	146.5	131.7	111.0	105.1	94.10	81.77
	After 48 h	158.9	114.4	100.8	93.42	87.08	59.20
	After 72 h	184.4	89.58	68.68	61.90	46.65	31.86

Control: DMSO.

Table 5
IC_{50} values for HL and L.

Compound	A172			LN229			NHA		
	24 h	48 h	72 h	24 h	48 h	72 h	24 h	48 h	72 h
HL	2.68 ± 0.19	0.95 ± 0.08	0.95 ± 0.08	9.55 ± 0.04	1.78 ± 0.05	0.85 ± 0.07	3.21 ± 0.04	0.64 ± 0.06	0.22 ± 0.04
L	1.9 ± 0.08	0.38 ± 0.05	0.27 ± 0.04	1.2 ± 0.05	0.57 ± 0.03	0.27 ± 0.05	3.29 ± 0.28	1.82 ± 0.33	0.43 ± 0.41
MPT (200 nM)	0.45 ± 0.09	0.44 ± 0.13	0.43 ± 0.09	0.448 ± 0.3	0.447 ± 0.01	.44 ± 0.07	0.49 ± 0.03	0.47 ± 0.04	0.45 ± 0.04

MPT: (Methylprophyl tryptamine) ($\overline{X}$ ± SD).

playing a crucial role in stopping reactive oxygen species (ROS) generation thereby offering advantageous affects as chemotherapeutic agents [36].

Fig. 3(a) and 4(a) show the comparative anti-glioblastomal activities of HL and L against A172 human glioblastoma cells. Cell viabilities in both the tested compounds reveal dose and time dependencies. At 0.16 μM cell viability for the deprotonated dicoumarol performs better than the protonated salt for A172 gliomas. In both cases the viability was significantly reduced by 50–60% and this trend remained almost constant at all concentrations. In the time dependent tests both the compounds showed a decrease in viability at the respective concentrations. After 72 h the cells were almost dead with the protonated derivative whereas, the deprotonated salt L reveal activity at high concentrations. Therefore, it can be tentatively deduced that the HL is cytotoxic to glioblastoma as well as living cells whereas, in comparison the L is somewhat more selective in proliferation and reveals activity at low concentration. This conclusion has been drawn by comparing the viabilities at different concentrations for normal human cell lines (NHA). The viability for HL is more than the viability shown by L derivative for NHA cells as shown in Table 4.

A similar behavior was observed when testing these two compounds against LN229 glioblastoma cells. Both compounds performed well against LN229 cells and almost similar behavior was observed in viabilities as shown in A172 cells. The deprotonated salt L is revealing better results at high concentration than shown by the same compound for A172 cells. Here again the time dependent behavior of the two compounds revealed that L performs well compared to the parent ligand HL where after 72 h the viabilities drop to almost zero. It can be deduced that at low concentrations HL shows better viability than L salt (probably, in part, by exposing the active sites of the coumarin framework for reaction with the cancerous cells where they are fully involved in hydrogen bonding in L). The

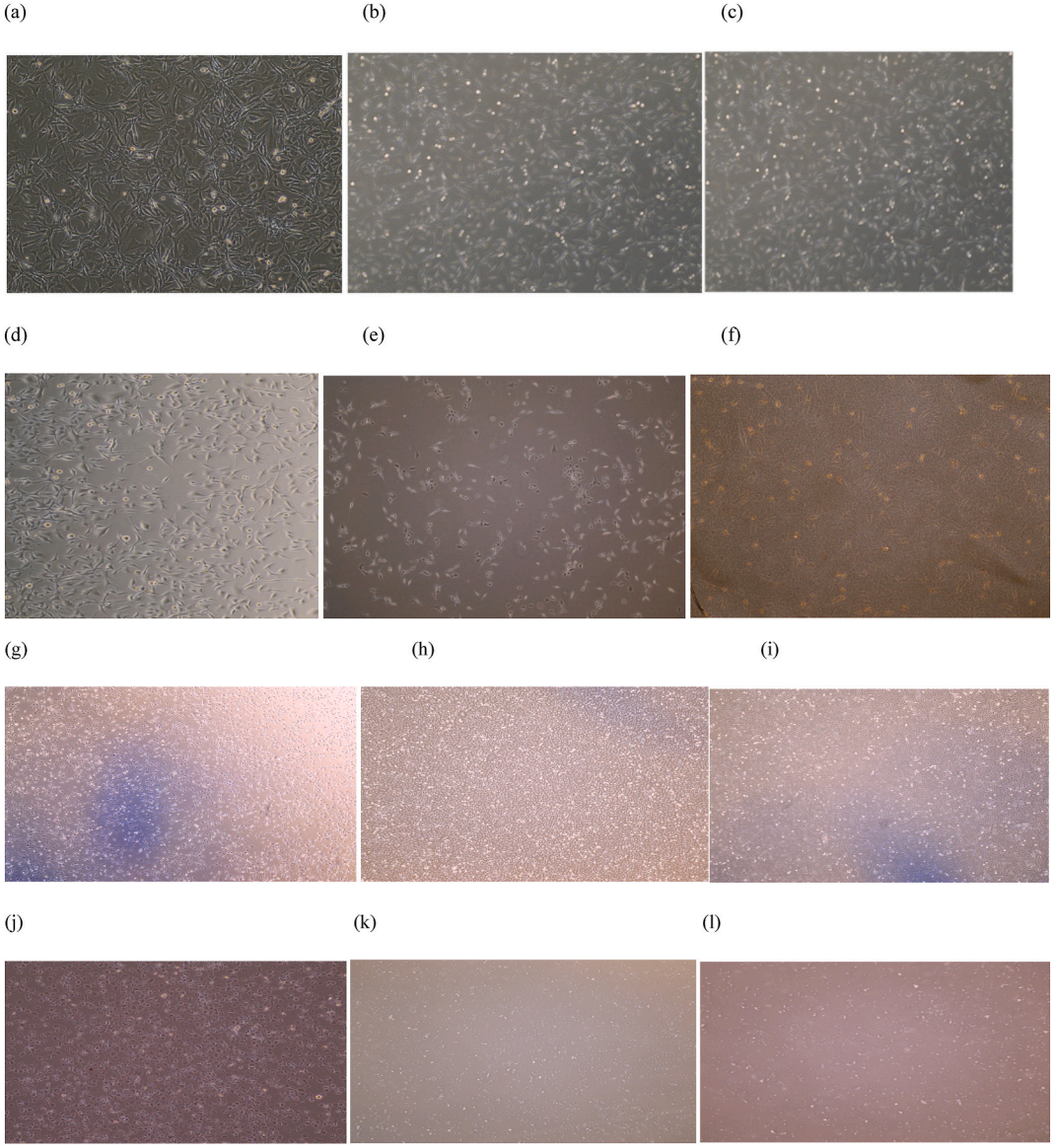

Fig. 5. The morphological change of A172, LN229 cells was observed by phase contrast microscope (magnification, × 200). (a) DMSO + 0 nm of HL against A172 (b) 160 nm of HL against A172 (c) 800 nm of HL against A172 (d) 4 μM of HL against A172 (e) 20 μM of HL against A172 (f) 100 μM of HL against A172 (g) DMSO + 0 nm of HL against LN229 (h) 160 nm of HL against LN229 (i) 800 nm of HL against LN229 (j) 4 μM of HL against LN229 (k) 20 μM of HL against LN229 (l) 100 μM of HL against LN229.

dose dependent behavior against LN229 is also notably distinct between the two compounds. Here the HL showed decreased viability at higher concentration. In contrast for L the viability halved at high dose concentrations. The best conclusion by comparing the results of both the synthesized compounds can be drawn by comparing the results for NHA cells. At high concentrations the viability for HL drops to almost zero whereas, the L show some activity thereby, making the L compound potentially better choice for the possible treatment of A172 and LN229.

IC_{50} values were calculated from the dose-response curves at various periods of time as shown in Table 5. The IC_{50} value for HL against A172 cells after 24 h is 2.68 μM and steadily decreases to 0.95 μM after 72 h. Similarly, for the same cell line the deprotonated L derivative showed an IC_{50} value of 1.9 μM after 24 h which decreased to 0.27 μM after 72 h. The IC_{50} values of both these compounds against LN229 glioma cells are also shown in Table 5. Again, the deprotonated L derivative performed well against LN229 with 24 h exposure and showed an IC_{50} value of 1.2 μM. The HL in comparison showed an IC_{50} value of 9.552 μM for the same time span. Upon extending the exposure duration of the compounds against LN229 cells it was seen that L performed better with an IC_{50} value of 0.27 μM after 72 h in comparison to HL with an 0.85 μM IC_{50} value.

The morphological changes of A172 and LN229 cells, such as the cell shrinking and decrease in cell number, further confirmed this

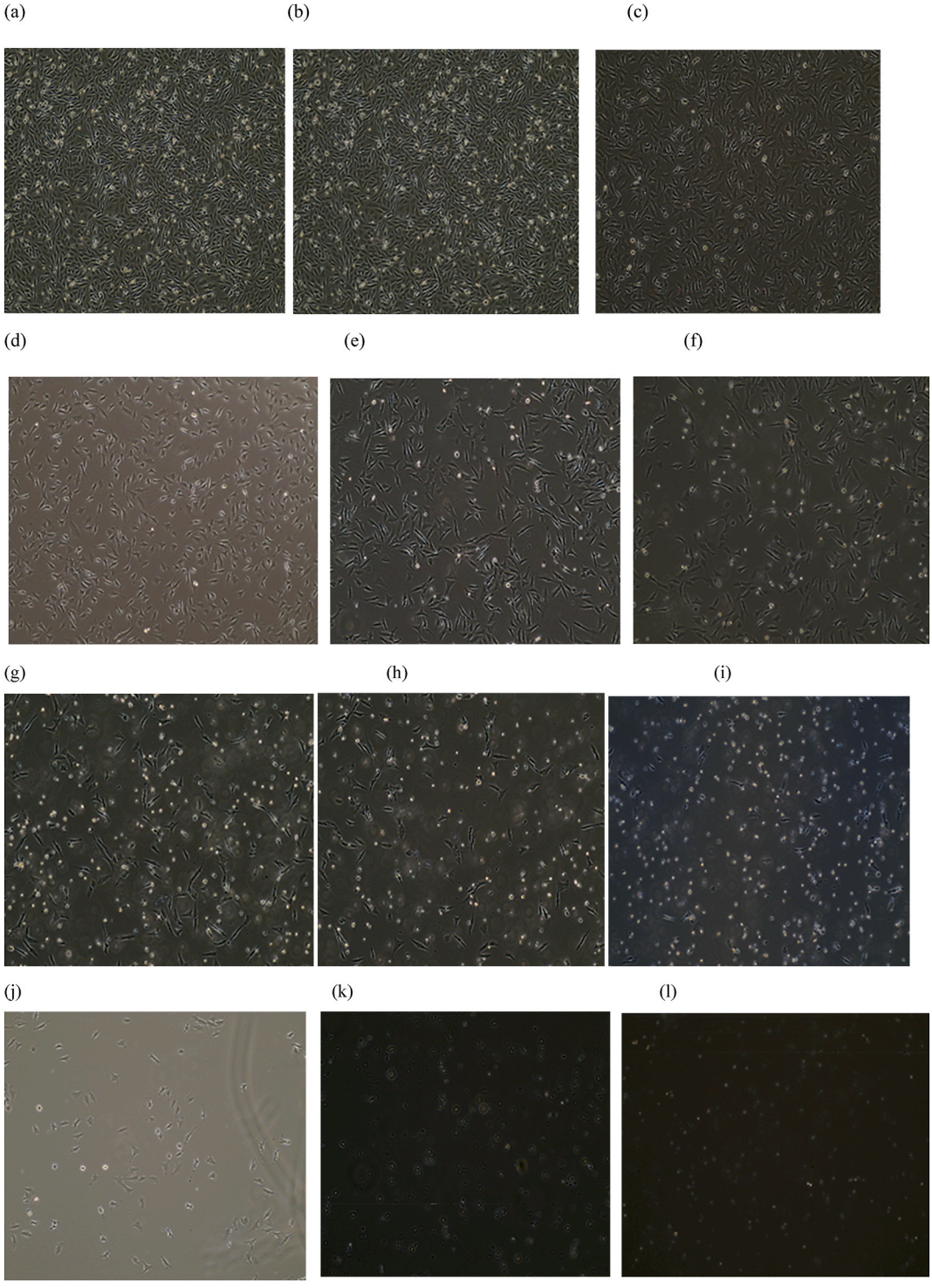

Fig. 6. The morphological change of A172, LN229 cells was observed by phase contrast microscope (magnification, × 200). (a) DMSO + 0 nm of L against A172 (b) 160 nm of L against A172 (c) 800 nm of L against A172 (d) 4 μM of L against A172 (e) 20 μM of L against A172 (f) 100 μM of L against A172 (g) DMSO + 0 nm of L against LN229 (h) 160 nm of L against LN229 (i) 800 nm of L against LN229 (j) 4 μM of L against LN229 (k) 20 μM of L against LN229 (l) 100 μM of L against LN229.

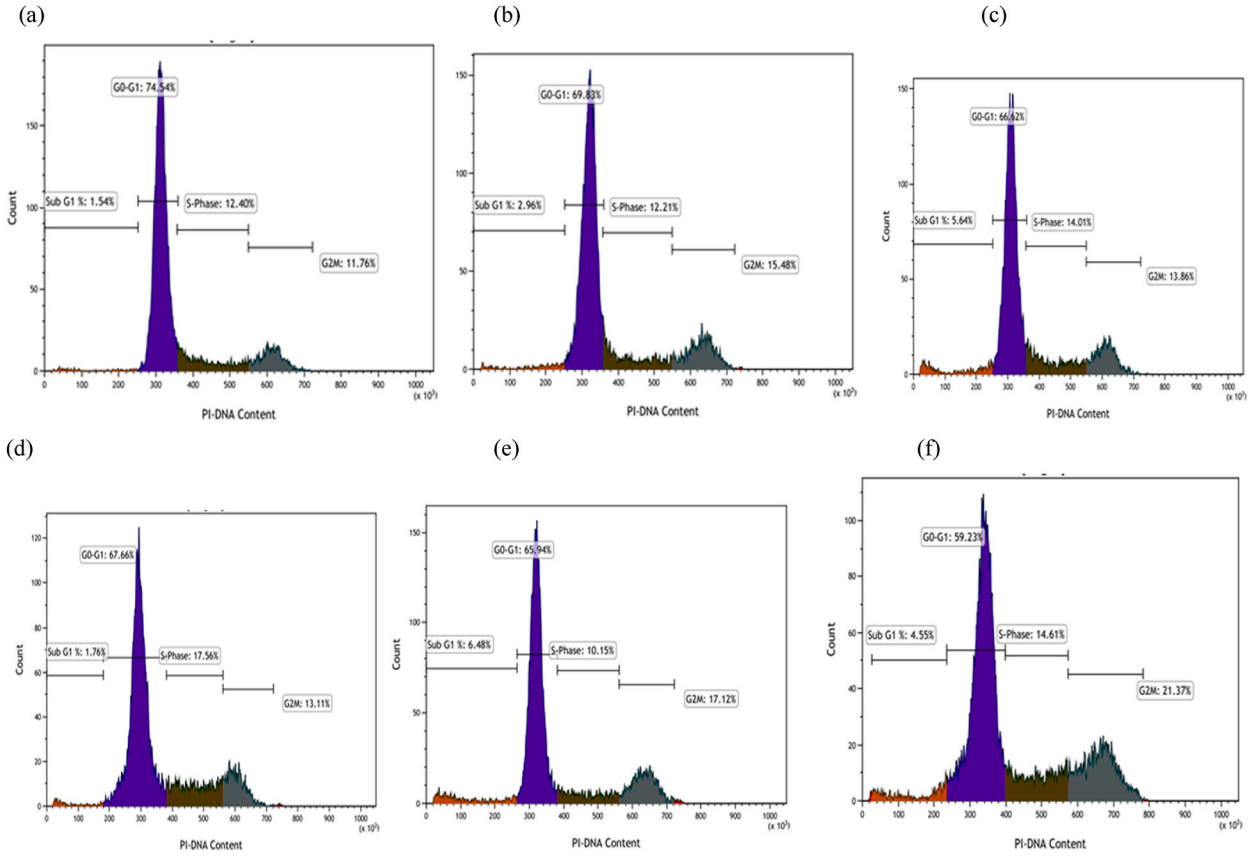

Fig. 7. Flow cytometric analysis of HL on A172 cell cycle and sub-G1 group. A: representative profiles of cell cycle. B: percentage of cells in various phases. Data represents mean ± S.D. of three experiments. *Significant differences between coumarin-treated cells and control *$p < 0.05$ (a) Untreated blank A172 cells after 24 h (b) Untreated blank A172 cells after 48 h (c) Untreated blank A172 cells after 72 h (d) 4 μM of HL after 24 h against A172 (e) 4 μM of HL after 48 h against A172 (f) 4 μM of HL after 72 h against A172.

effect (Figs. 5 and 6). Given that, in both the coumarin derivatives, the deprotonated L salt showed more cytotoxicity for A172 and LN229 than the NHA cells.

3.3. Cell cycle arrest and apoptosis

Flow cytometry was used to investigate if apoptosis or/and cell cycle arrest were involved in L-induced cell growth inhibition against human glioblastoma. Thereby, both the synthesized derivatives were tested for flow cytometry analysis.

Compound HL flow cytometry graphs for A172 cells (Fig. 7) after treatment with 4 μM dose show that the cell cycle arrest was caused at G0/G1 phase cell cycle. The time dependent studies revealed that the percentage in this phase was significantly reduced from 67.66% to 59.23%. The sub G1 phase also appeared with percentage of about 1.76% after 24 h and steadily increases to 6.48% after 48 h. After 72 h the value of percentage dopped again to 4.55%. This sudden drop may be due to apoptosis induced by dicoumarol. Similarly, the flow cytometry analysis for compound HL against LN229 (Fig. 8) reveal that G0/G1 phase cell cycle was reduced to 70.33% after 24 h. As the exposure time increases this percentage also goes down and reaches to 61.70% after 48 h. Whereas, after 72 h a tremendous decrease was observed with percentage of 41.11%. Comparing the results of compound HL against A172 and LN229 it may clearly be deduced that LN229 cells were arrested at G0/G1 phase cell cycle more successfully than A172 cells. Compound HL also enhanced the percentages of other phases of cell cycle arrest as well.

Compound L significantly caused G0/G1 phase cell cycle arrest in A172 and LN229 cells after at different time, as illustrated in Figs. 9 and 10. Compound L (10 μM) against A172 cells showed a significant decrease in G0/G1 phase percentage from 79.26, 69.83, and 68.67 at various exposure time. The sub-G1 groups also appeared in the cell cycle at 2.28, 8.51, and 14.43%.

Similarly, the flow cytometric results of LN229 were found more promising than A172 cells. The percentage of cells in G0/G1 decreased from 72.83, 74.54, and 76.90% to 6.71, 70.55 and 47.34% respectively. Similarly, in the cell cycle of sub-G1 group the percentages of 8.19, 6.12 and 32.70 appeared indicating that coumarin induced apoptosis. These findings clearly illustrated that inducing G0/G1 phase cell cycle arrest played a significant role in the L-mediated anticancer mechanism.

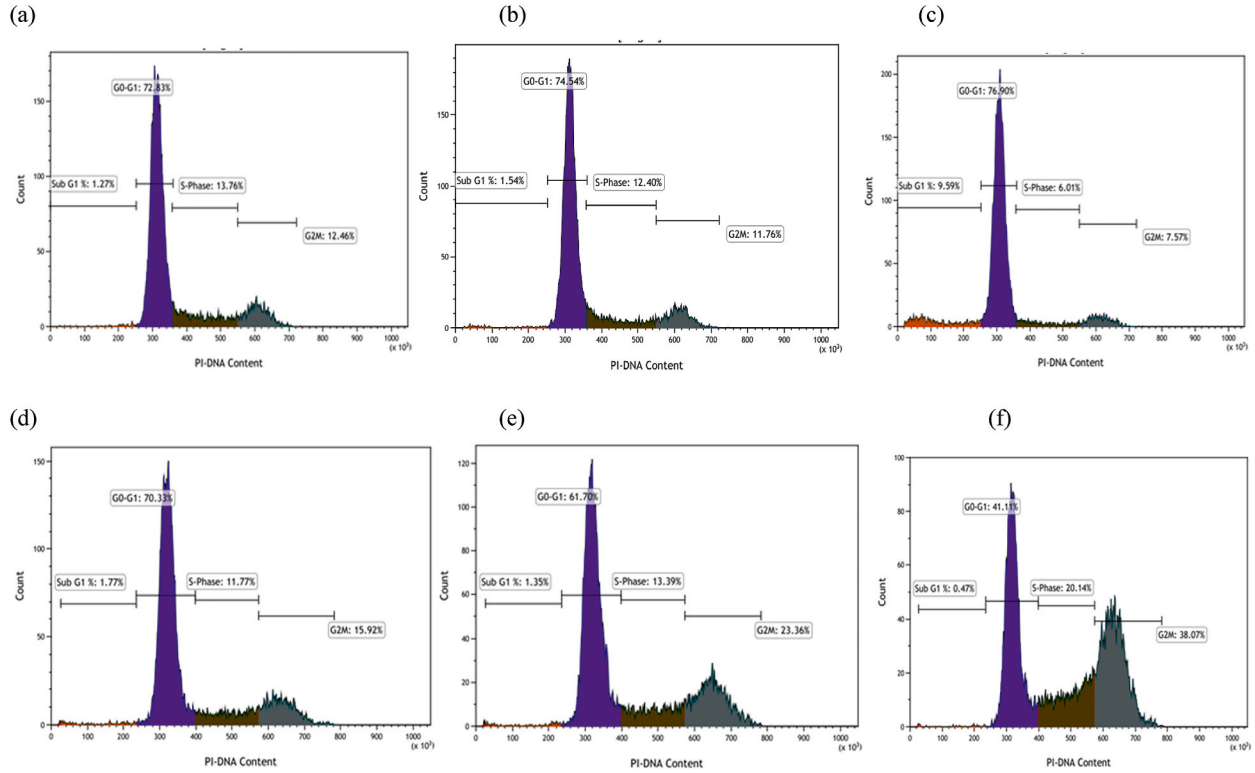

Fig. 8. Flow cytometric analysis of HL on LN229 cell cycle and sub-G1 group. A: representative profiles of cell cycle. B: percentage of cells in various phases. Data represents mean ± S.D. of three experiments. *Significant differences between coumarin-treated cells and control *$p < 0.05$ (a) Untreated blank LN229 cells after 24 h (b) Untreated blank LN229 cells after 48 h (c) Untreated blank LN229 cells after 72 h (d) 4 μM of HL after 24 h against LN229 (e) 4 μM of HL after 48 h against LN229 (f) 4 μM of HL after 72 h against LN229.

3.4. DPPH scavenging assay

Antioxidants are the molecular motifs capable of donating electrons or hydrogen atoms to bring structural modifications ultimately stops the radical property and hence cellular oxidative damage is reduced [36]. Inside biological systems two types of antioxidants exist viz; natural and synthetic. Natural antioxidants glutathione, Uric acid, vitamin C, vitamin E, β-carotene, Ubiquinol and some enzyme like SOD's whereas many synthetic antioxidants have been reported so far including sole organic and metal coordinated derivatives [37–39]. Antioxidants are added industrially to value added items to enhance shelf life. Previous studies conclude that antioxidants are singlet oxygen quencher, hydrogen donor and peroxide decomposers [40]. Reactive oxygen species (ROS) or free radicals are sensitive and short-lived chemical species which have one or more unpaired electron capable of independent existence. They are produced because of usual cellular metabolic activities occurring inside mitochondria. ROS are peroxides, singlet oxygen, hydroxyl radicals, superoxide ions, nitric oxide and peroxy nitrates. All these free radicals may belong to endogenous or exogenous. ROS generation inside cancer cells is playing pathogenic role leading to degenerative diseases [41]. Therefore, a compound with hybrid functionalities i.e., showing both cancer and antioxidant properties, may pave its way for a better option toward the anticancer drug development.

Basing this hypothesis, the synthesized coumarin derivatives were also tested for their possible free radical scavenging properties. The results were compared with ascorbic acid taken as standard (Table 6). Both the compounds were studied dose dependently over the concentration range of 250–1000 μM/mL. Compound HL shown percentage of 10.37 ± 0.08 over the concentration of 250 μM/mL and it reaches to 25.62 ± 0.07 over the concentration of 1000 μg/mL with $IC_{50} = 342.1 \pm 0.01$ μM/mL. The deprotonated derivative L shown percentage range of 22.68 ± 0.01 to 37.03 ± 0.07 over the concentration ranges of 250–1000 μgM/ml. IC_{50} value for compound L was to be 197.4 ± 0.06 μM/mL comparatively less than compound HL. By comparing these results with vitamin C as a standard with $IC_{50} = 89.2 \pm 0.334$ μM/mL, it can be deduced that the deprotonated derivative will behave better than the parent dicoumarol. The reason coined for the better activity of deprotonated derivative might be due to the availability of lactone oxygen atoms for abstraction of protons where these protons are involved in intramolecular hydrogen bonding in the parent dicoumarol.

4. Conclusion

A dicoumarol derivative 3,3′-[(4-methoxyphenyl)methanediyl]bis(4-hydroxy-2Hchromen-2-one) (HL) was deprotonated to its

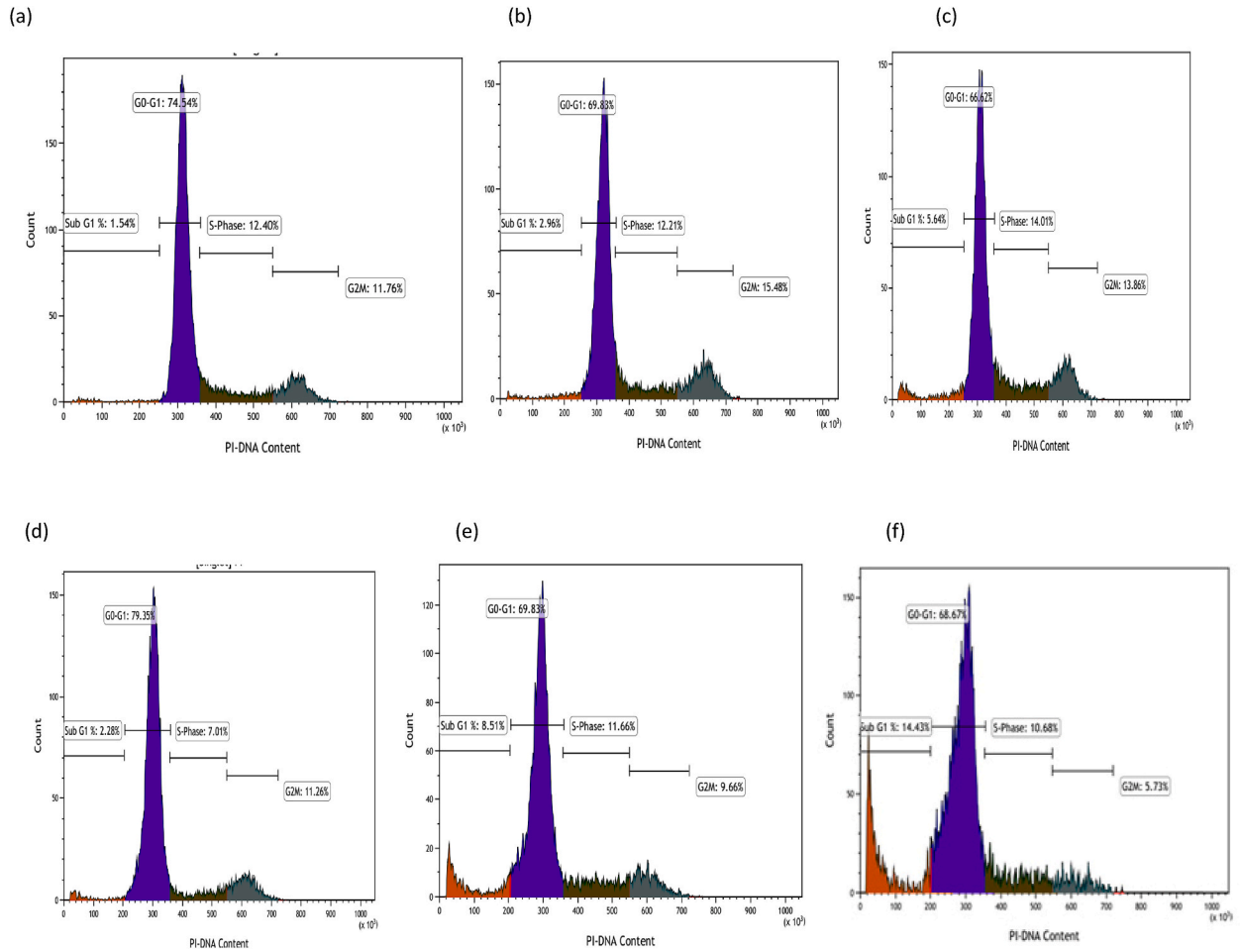

Fig. 9. Flow cytometric analysis of L on A172 cell cycle and sub-G1 group. A: representative profiles of cell cycle. B: percentage of cells in various phases. Data represents mean ± S.D. of three experiments. *Significant differences between coumarin-treated cells and control *$p < 0.05$ A172 (a) Untreated blank A172 cells after 24 h (b) Untreated blank A172 cells after 48 h (c) Untreated blank A172 cells after 72 h (d) 4 μM of L after 24 h against A172 (e) 4 μM of L after 48 h against A172 (f) 4 μM of L after 72 h against A172.

triethylammonium salt {triethylammonium-3-[(4-methoxyphenyl)(4-hydroxy-2-oxo-2H-chromen-3-yl)methyl]-2-oxo-2H-chromen-4-olate (L)}. Both the compounds were characterized using spectroscopic and analytical techniques. Compound L was crystallized in Monoclinic, *P21/n* crystal system. The inter and intramolecular hydrogen bonding were extensively found in the crystal system of L and are responsible for decreasing the steric strain caused by deprotonation. The in vitro antiglioblastoma activity for both the synthesized compounds were studied against A172 and LN229 glioma cells. The results were compared with the cytotoxicity of both the compounds with the normal human astrocytes (NHA). Time and dose dependent studies were performed against all the tested cells. The cell viability studies of both the compounds against A172 cells confirmed that compound HL is more cytotoxic at high concentrations to the exposed cells as well as NHA cells. In comparison to it, compound L show less cytotoxicity against A172 cells but its exposure to NHA cells reveal promising results. Similarly, both the compounds against LN229 cells shown similar behavior and revealed that compound L performed better than HL. The IC_{50} value of HL against A172 lies within the range 2.68–0.24 μM and for L this range was found to be 1.9–0.27 μM. Similarly, against LN229 cells IC_{50} values for HL varies within the range 1.277–0.266 μM and for L it is 9.552–0.847 μM. The mechanism of apoptosis was studied by flow cytometry which revealed that both the compounds are causing apoptosis in G0/G1 and Sub G1 phases. Antioxidant activity of synthesized compounds was also investigated using DPPH free radicals The results revealed that compound L was involved in scavenging DPPH free radicals better than compound HL. Overall, the effectiveness of these compounds can be utilized to design significant anticancer agents against glioblastoma cancer. Further, research is required to study some other deprotonated derivatives to search for a better option (if exist) against A172 and LN229 gliomas.

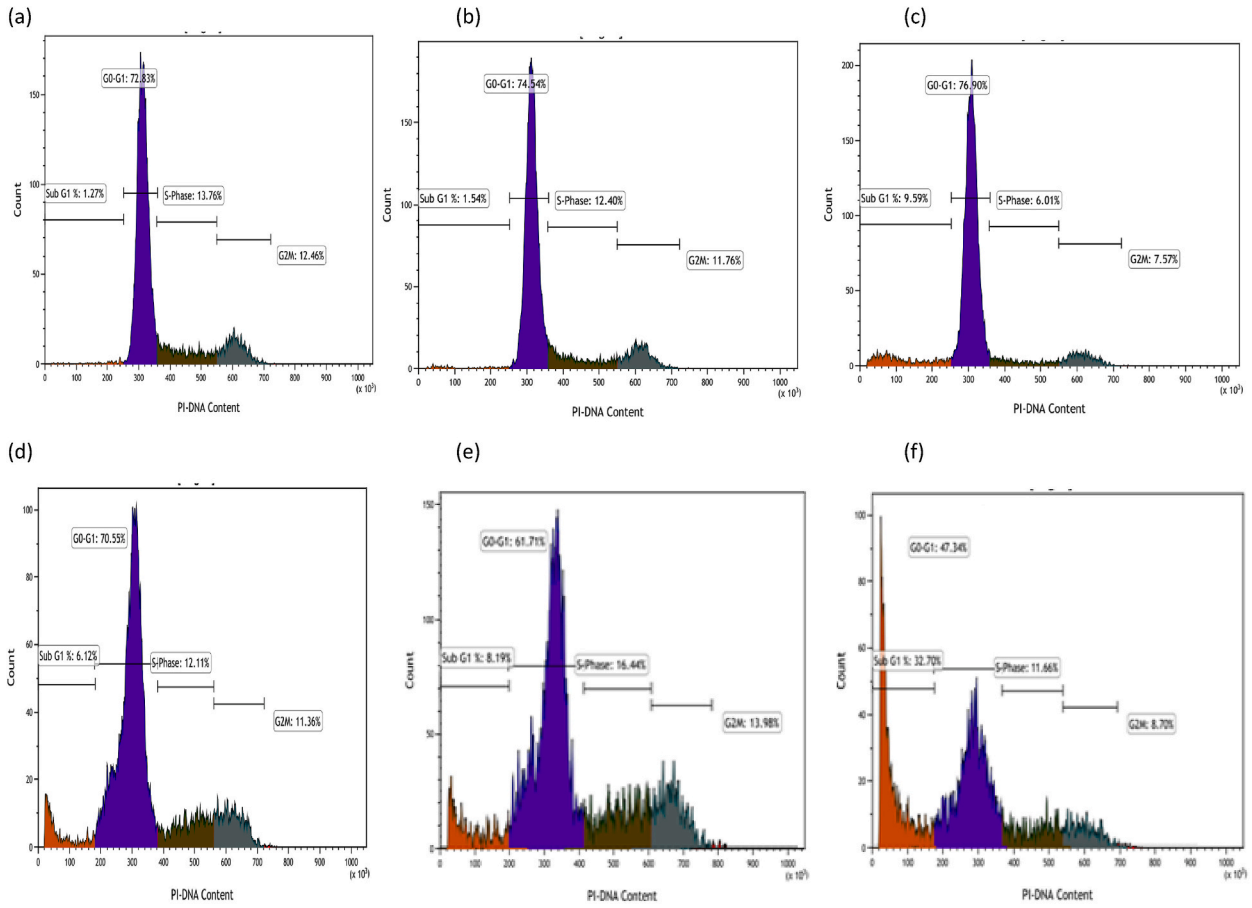

Fig. 10. Flow cytometric analysis of L on LN229 cell cycle and sub-G1 group. A: representative profiles of cell cycle. B: percentage of cells in various phases. Data represents mean ± S.D. of three experiments. *Significant differences between coumarin-treated cells and control *$p < 0.05$ (a) Untreated blank LN229 cells after 24 h (b) Untreated blank LN229 cells after 24 h (c) Untreated blank LN229 cells after 24 h (d) 10 μM of L after 24 h against LN229 (e) 10 μM of L after 48 h against LN229 (f) 10 μM of L after 72 h against LN229.

Table 6
DPPH scavenging activities of HL and L.

Compound	Percentage of antioxidant activity				IC_{50} (μM/mL)
	250 μM/mL	**500** μM/mL	**750** μM/mL	**1000** μM/mL	
HL	10.37 ± 0.08	15.12 ± 0.03	19.41 ± 0.02	25.62 ± 0.07	342.1 ± 0.014
L	22.68 ± 0.01	27.29 ± 0.06	32.93 ± 0.03	37.03 ± 0.07	197.4 ± 0.06
Control_+Ascorbic acid	74.08 ± 0.04	80.24 ± 0.01	85.79 ± 0.1	92.059 ± 0.08	89.2 ± 0.33

Declarations

Author contributions statement

Muhammad Ikram: Conceived and designed the experiments; Performed the experiments; Analyzed and interpreted the data; Contributed reagents, materials, analysis tools or data; Wrote the paper.

Sadia Rehman; Conceived and designed the experiments; Contributed reagents, materials, analysis tools or data; Wrote the paper.

Rizwan Khan: Performed the experiments; Analyzed and interpreted the data; Wrote the paper.

Vinay K. Puduvalli: Performed the experiments; Analyzed and interpreted the data; Contributed reagents, materials, analysis tools or data.

Fawaz Alasmari; Abdullah F AlAsmari: Analyzed and interpreted the data; Performed the experiments.

Momin Khan: Contributed reagents, materials, analysis tools or data.

Afzal Khan: Analyzed and interpreted the data; Contributed reagents, materials, analysis tools or data; Wrote the paper.

Data availability statement

Data will be made available upon request.

Declaration of competing interest

The authors declare that they have no known competing financial interests or personal relationships that could have appeared to influence the work reported in this paper.

Acknowledgments

This work was supported by the Researchers supporting project number (RSP2023R235), King Saud University, Riyadh, Saudi Arabia. This research was supported by grants from the Higher Education Commission Pakistan {NRPU sponsored project no. Ref No. 20-14898/NRPU/R&D/HEC/2021-2020}, Abdul Wali Khan University Mardan Pakistan and MD Anderson cancer center at the University of Texas, USA.

Appendix A. Supplementary data

Supplementary data to this article can be found online at https://doi.org/10.1016/j.heliyon.2023.e17601.

References

[1] E. Izycka-Swieszewska, E. Bien, J. Stefanowicz, E. Szurowska, E. Szutowicz-Zielinska, M. Koczkowska, D. Sigorski, W. Kloc, W. Rogowski, E. Adamkiewicz-Drozynska, Malignant gliomas as second neoplasms in pediatric cancer survivors: neuropathological study, BioMed Res. Int. 2018 (2018) 1–10, https://doi.org/10.1155/2018/4596812.

[2] M.W. Chen, A.A. Morsy, S. Liang, W.H. Ng, Re-Do craniotomy for recurrent Grade IV glioblastomas: impact and outcomes from the national neuroscience institute Singapore, World Neurosurg. 87 (2016) 439–445, https://doi.org/10.1016/j.wneu.2015.10.051.

[3] C. Birzu, P. French, M. Caccese, G. Cerretti, A. Idbaih, V. Zagonel, G. Lombardi, Recurrent glioblastoma: from molecular landscape to new treatment perspectives, Cancers (Basel) 13 (2020) 47, https://doi.org/10.3390/cancers13010047.

[4] M. Butnariu, C. Quispe, N. Koirala, S. Khadka, C.M. Salgado-Castillo, M. Akram, R. Anum, B. Yeskaliyeva, N. Cruz-Martins, M. Martorell, M. Kumar, R. Vasile Bagiu, A.F. Abdull Razis, U. Sunusi, R. Muhammad Kamal, J. Sharifi-Rad, Bioactive effects of curcumin in human immunodeficiency virus infection along with the most effective isolation techniques and type of nanoformulations, Int. J. Nanomed. 17 (2022) 3619–3632, https://doi.org/10.2147/IJN.S364501.

[5] V.L.M. Silva, R. Silva-Reis, A. Moreira-Pais, T. Ferreira, P.A. Oliveira, R. Ferreira, S.M. Cardoso, J. Sharifi-Rad, M. Butnariu, M.A. Costea, I. Grozea, Dicoumarol: from chemistry to antitumor benefits, Chin. Med. 17 (2022) 145, https://doi.org/10.1186/s13020-022-00699-0.

[6] R. Flašík, H. Stankovičová, A. Gáplovský, J. Donovalová, Synthesis and study of novel coumarin derivatives potentially utilizable as memory Media, Molecules 14 (2009) 4838–4848, https://doi.org/10.3390/molecules14124838.

[7] K. Venkata Sairam, B.M. Gurupadayya, R.S. Chandan, D.K. Nagesha, B. Vishwanathan, A review on chemical profile of coumarins and their therapeutic role in the treatment of cancer, Curr. Drug Deliv. 13 (2016) 186–201, https://doi.org/10.2174/1567201812666150702102800.

[8] A.A. Al-Amiery, R.I.H. Al-Bayati, K.Y. Saour, M.F. Radi, Cytotoxicity, antioxidant, and antimicrobial activities of novel 2-quinolone derivatives derived from coumarin, Res. Chem. Intermed. 38 (2012) 559–569, https://doi.org/10.1007/s11164-011-0371-2.

[9] V.S.V. Satyanarayana, P. Sreevani, A. Sivakumar, V. Vijayakumar, Synthesis and antimicrobial activity of new Schiff bases containing coumarin moiety and their spectral characterization, Arkivoc 2008 (2009) 221–233, https://doi.org/10.3998/ark.5550190.0009.h21.

[10] A. Kotali, I.S. Lafazanis, P.A. Harris, Synthesis of 6,7-diacylcoumarins via the transformation of a hydroxy into a carbonyl group, Synth. Commun. 38 (2008) 3996–4006, https://doi.org/10.1080/00397910802250911.

[11] S. Kawaii, Y. Tomono, K. Ogawa, M. Sugiura, M. Yano, Y. Yoshizawa, C. Ito, H. Furukawa, Antiproliferative effect of isopentenylated coumarins on several cancer cell lines, Anticancer Res. 21 (2001) 1905–1911.

[12] M.E. Marshall, K. Kervin, C. Benefield, A. Umerani, S. Albainy-Jenei, Q. Zhao, M.B. Khazaeli, Growth-inhibitory effects of coumarin (1,2-benzopyrone) and 7-hydroxycoumarin on human malignant cell lines in vitro, J. Cancer Res. Clin. Oncol. 120 (1994) S3–S10, https://doi.org/10.1007/BF01377114.

[13] R.B. Myers, M. Parker, W.E. Grizzle, The effects of coumarin and suramin on the growth of malignant renal and prostatic cell lines, J. Cancer Res. Clin. Oncol. 120 (1994) S11–S13, https://doi.org/10.1007/BF01377115.

[14] J.S. Lopez-Gonzalez, H. Prado-Garcia, D. Aguilar-Cazares, J.A. Molina-Guarneros, J. Morales-Fuentes, J.J. Mandoki, Apoptosis and cell cycle disturbances induced by coumarin and 7-hydroxycoumarin on human lung carcinoma cell lines, Lung Cancer 43 (2004) 275–283, https://doi.org/10.1016/j.lungcan.2003.09.005.

[15] G.B. Lim, Warfarin: from rat poison to clinical use, Nat. Rev. Cardiol. (2017), https://doi.org/10.1038/nrcardio.2017.172.

[16] B.R. Kusuma, A. Khandelwal, W. Gu, D. Brown, W. Liu, G. Vielhauer, J. Holzbeierlein, B.S.J. Blagg, Synthesis and biological evaluation of coumarin replacements of novobiocin as Hsp90 inhibitors, Bioorg. Med. Chem. 22 (2014) 1441–1449, https://doi.org/10.1016/j.bmc.2013.12.056.

[17] A.R. Verma, M. Vijayakumar, C.V. Rao, C.S. Mathela, In vitro and in vivo antioxidant properties and DNA damage protective activity of green fruit of Ficus glomerata, Food Chem. Toxicol. 48 (2010) 704–709, https://doi.org/10.1016/j.fct.2009.11.052.

[18] C.G. Arya, R. Gondru, Y. Li, J. Banothu, Coumarin–benzimidazole hybrids: a review of developments in medicinal chemistry, Eur. J. Med. Chem. 227 (2022), 113921, https://doi.org/10.1016/j.ejmech.2021.113921.

[19] G.M. Sheldrick, *SHELXT* – integrated space-group and crystal-structure determination, Acta Crystallogr. A Found. Adv. 71 (2015) 3–8, https://doi.org/10.1107/S2053273314026370.

[20] L.J. Farrugia, *WinGX* and *ORTEP for Windows* : an update, J. Appl. Crystallogr. 45 (2012) 849–854, https://doi.org/10.1107/S0021889812029111.

[21] G.M. Sheldrick, Crystal structure refinement with *SHELXL*, Acta Crystallogr. C Struct. Chem. 71 (2015) 3–8, https://doi.org/10.1107/S2053229614024218.

[22] S.-P. Han, J.-H. Kim, M.-E. Han, H.-E. Sim, K.-S. Kim, S. Yoon, S.-Y. Baek, B.-S. Kim, S.-O. Oh, SNAI1 is involved in the proliferation and migration of glioblastoma cells, Cell. Mol. Neurobiol. 31 (2011) 489–496, https://doi.org/10.1007/s10571-010-9643-4.

[23] C.-C. Su, G.-W. Chen, J.-G. Lin, L.-T. Wu, J.-G. Chung, Curcumin inhibits cell migration of human colon cancer colo 205 cells through the inhibition of nuclear factor kappa B/p65 and down-regulates cyclooxygenase-2 and matrix metalloproteinase-2 expressions, Anticancer Res. 26 (2006) 1281–1288.

[24] S.-J. Zhao, X.-J. Wang, Q.-J. Wu, C. Liu, D.-W. Li, X.-T. Fu, H.-F. Zhang, L.-R. Shao, J.-Y. Sun, B.-L. Sun, J. Zhai, C.-D. Fan, Induction of G1 cell cycle arrest in human glioma cells by salinomycin through triggering ROS-mediated DNA damage in vitro and in vivo, Neurochem. Res. 42 (2017) 997–1005, https://doi.org/10.1007/s11064-016-2132-5.

[25] J.R. Soare, T.C.P. Dinis, A.P. Cunha, L. Almeida, Antioxidant activities of some extracts of *Thymus zygis*, Free Radic. Res. 26 (1997) 469–478, https://doi.org/10.3109/10715769709084484.

[26] S. Rehman, M. Ikram, R.J. Baker, M. Zubair, E. Azad, S. Min, K. Riaz, K. Mok, S.-U. Rehman, Synthesis, characterization, in vitro antimicrobial, and U2OS tumoricidal activities of different coumarin derivatives, BMC Chem. 7 (2013) 68, https://doi.org/10.1186/1752-153X-7-68.

[27] R. Bengiat, M. Gil, A. Klein, B. Bogoslavsky, S. Cohen, J. Almog, Bis(benzyltrimethylammonium) bis[(4 *SR* ,12 *SR* ,18 *RS* ,26 *RS*)-4,18,26-trihydroxy-12-oxido-13,17-dioxaheptacyclo[14.10.0.0 ^{3,14} .0 ^{4,12} .0 ^{6,11} .0 ^{18,26} .0 ^{19,24}]hexacosa-1,3(14),6,8,10,15,19,21,23-nonaene-5,25-dione] sesquihydrate: dimeric structure formation *via* [O–H–O]$^{-}$ *negative charge-assisted hydrogen bonds (–CAHB)* with benzyltrimethylammonium counter-ions, Acta Crystallogr. E Crystallogr. Commun. 72 (2016) 399–402, https://doi.org/10.1107/S2056989016002899.

[28] M. Ikram, S. Rehman, A. Khan, C. Schulzke, Crystal structure of the tri-ethyl-ammonium salt of 3-[(4-hy-droxy-3-meth-oxy-phen-yl)(4-hy-droxy-2-oxo-2H-chromen-3-yl)meth-yl]-2-oxo-2H-chromen-4-olate, Acta Crystallogr. E Crystallogr. Commun. 74 (2018) 282–286, https://doi.org/10.1107/S2056989018001561.

[29] M. Waheed, N. Ahmed, Coumarin based novel ligands in the Suzuki–Miyaura and Mizoroki–Heck cross-couplings under aqueous medium, Tetrahedron Lett. 57 (2016) 3785–3789, https://doi.org/10.1016/j.tetlet.2016.07.028.

[30] S. Stanchev, G. Momekov, F. Jensen, I. Manolov, Synthesis, computational study and cytotoxic activity of new 4-hydroxycoumarin derivatives, Eur. J. Med. Chem. 43 (2008) 694–706, https://doi.org/10.1016/j.ejmech.2007.05.005.

[31] R.D. Thornes, L. Daly, G. Lynch, B. Breslin, H. Browne, H.Y. Browne, T. Corrigan, P. Daly, G. Edwards, E. Gaffney, J. Henley, T. Healy, F. Keane, F. Lennon, N. McMurray, S. O'Loughlin, M. Shine, A. Tanner, Treatment with coumarin to prevent or delay recurrence of malignant melanoma, J. Cancer Res. Clin. Oncol. 120 (1994) S32–S34, https://doi.org/10.1007/BF01377122.

[32] E. Budzisz, Cytotoxic effects, alkylating properties and molecular modelling of coumarin derivatives and their phosphonic analogues, Eur. J. Med. Chem. 38 (2003) 597–603, https://doi.org/10.1016/S0223-5234(03)00086-2.

[33] R.D. Thornes, G. Lynch, M.V. Sheehan, Cimetidine and coumarin therapy of melanoma, Lancet 320 (1982) 328, https://doi.org/10.1016/S0140-6736(82)90295-1.

[34] F.H. Dexeus, C.J. Logothetis, A. Sella, K. Fitz, R. Amato, J.M. Reuben, N. Dozier, Phase II study of coumarin and cimetidine in patients with metastatic renal cell carcinoma, J. Clin. Oncol. 8 (1990) 325–329, https://doi.org/10.1200/JCO.1990.8.2.325.

[35] O. Kokron, S. Maca, G. Gasser, P.R. Schmidt, Cimetidine and coumarin therapy of renal cell carcinoma, Oncology 48 (1991) 102–106, https://doi.org/10.1159/000226905.

[36] W. Brand-Williams, M.E. Cuvelier, C. Berset, Use of a free radical method to evaluate antioxidant activity, LWT - Food Sci. Technol. 28 (1995) 25–30, https://doi.org/10.1016/S0023-6438(95)80008-5.

[37] C. Kerksick, D. Willoughby, The antioxidant role of glutathione and N-acetyl-cysteine supplements and exercise-induced oxidative stress, J. Int. Soc. Sports Nutr. 2 (2005), https://doi.org/10.1186/1550-2783-2-2-38.

[38] Y.Y. Sautin, R.J. Johnson, Uric acid: the oxidant-antioxidant paradox, Nucleos Nucleot. Nucleic Acids 27 (2008) 608–619, https://doi.org/10.1080/15257770802138558.

[39] T.C. Mosha, H.E. Gaga, R.D. Pace, H.S. Laswai, K. Mtebe, Effect of blanching on the content of antinutritional factors in selected vegetables, Plant Foods Hum. Nutr. 47 (1995) 361–367, https://doi.org/10.1007/BF01088275.

[40] A. Krieger-Liszkay, Singlet oxygen production in photosynthesis, J. Exp. Bot. 56 (2005) 337–346, https://doi.org/10.1093/jxb/erh237.

[41] G. Lenaz, The mitochondrial production of reactive oxygen species: Mechanisms and implications in human pathology, IUBMB Life 52 (2001) 159–164, https://doi.org/10.1080/15216540152845957.